Laser & Photon. Rev. **2**, No. 6, 514–526 (2008) / **DOI** 10.1002/lpor.200810018

Abstract The quest for enhanced light-matter interactions has enabled a tremendous increase in the performance of photonic-crystal nanoresonators in the past decade. State-of-the-art nanocavities now offer mode lifetime in the nanosecond range with confinement volumes of a few hundredths of a cubic micrometer. These results are certainly a consequence of the rapid development of fabrication techniques and modeling tools at micro- and nanometric scales. For future applications and developments, it is necessary to deeply understand the intrinsic physical quantities that govern the photon confinement in these cavities. We present a review of the different physical mechanisms at work in the photon confinement of almost all modern PhC cavity constructs. The approach relies on a Fabry-Perot picture and emphasizes three intrinsic quantities, the mirror reflectance, the mirror penetration depth and the defect-mode group velocity, which are often hidden by global analysis relying on an a posteriori analysis of the calculated cavity mode. The discussion also includes nanoresonator constructs, such as the important micropillar cavity, for which some subtle scattering mechanisms significantly alter the Fabry-Perot picture.

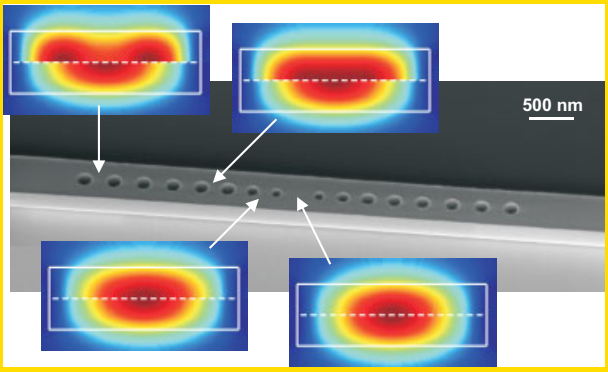

Photon lifetime in photonic crystal nanocavities is mainly limited by Bloch-mode profile mismatches, and by engineering the mirror termination, one may lower the mismatch and increase the lifetime.

Photon confinement in photonic crystal nanocavities

Philippe Lalanne *, *Christophe Sauvan and Jean Paul Hugonin*

Laboratoire Charles Fabry de l'Institut d'Optique, CNRS, University Paris-Sud, Campus Polytechnique, RD 128, 91127 Palaiseau, France

Received: 11 April 2008, Revised: 24 June 2008, Accepted: 15 July 2008
Published online: 3 September 2008

Key words: Nanocavity, Fabry-Perot resonator, slow waves, taper, photonic crystal, Bragg mirrors.

PACS: 42.60.Da, 42.55.Sa, 42.70.Qs, 42.50.Pq

1. Introduction

Ultrasmall microcavities that durably trap photons in small volumes close to the diffraction limit are essential components for modern optics and various related fields [1]. Although it is true that the physical phenomena observed in those cavities are similar to those previously reported in more conventional resonator etalons, microcavities allow the performance to be boosted by orders of magnitude and offer a reliable platform for dense integration. They are characterized by two main quantities: the mode volume V and the quality factor Q. The former represents the spatial extent of the electromagnetic confinement and the latter is proportional to the photon lifetime in the cavity. Thus Q and $1/V$ can be seen as the spectral and spatial energy density associated to the resonant mode, respectively. When trapped for sufficiently long times in a small space, photons strongly interact with the host material and thus create significant nonlinear [2], quantum [3] and optomechanical [4] effects, to quote only a few of them. The modification of the spontaneous emission rate of atoms placed in resonance with the microcavity mode is an emblematic effect [5].

During the last decade, the rapid development of fabrication techniques at micro- and nanometric scales has enabled the successful demonstration of various types of microresonators, such as disk-shaped or wire ring resonators, or photonic crystal (PhC) cavities, see [6] for an overview. Consequently, many physical phenomena have been observed with unprecedented compactness, integration and power thresholds, such as the Purcell effect [7], strong

* Corresponding author: e-mail: Philippe.Lalanne@institutoptique.fr

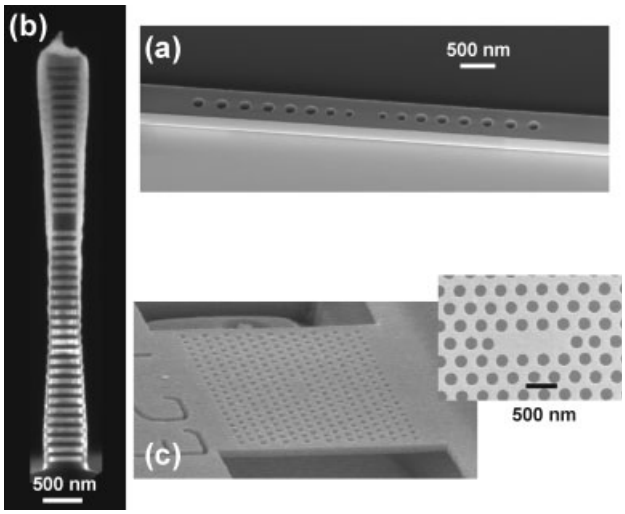

Figure 1 Different types of photonic crystal microcavities. (a) PhC cavity in a ridge waveguide in a silicon-on-insulator substrate (courtesy David Peyrade, Laboratoire des Technologies de la Microélectronique [26]). (b) GaAs/GaAlAs micropillar (courtesy Gilles Patriarche, Laboratoire de Photonique et de Nanostructures [23]). (c) L3 cavity in a 2D PhC etched in a GaAs membrane suspended in air (courtesy Sylvain Combrié, Thalès Research and Technology [29]).

coupling between quantum dot and cavity modes [8, 9], light storing [10], wavelength routing [11] and buffering [12], optical bistability [13], high-speed modulation in silicon [14, 15], lasing at ultralow thresholds [16–19] and single-molecule sensing [20]. Total internal reflection is solely exploited in disk-shaped or wire ring resonators, but a hybrid confinement that combines photonic bandgaps in one or two dimensions with index guiding is exploited in PhC microcavities such as micropillars [21–23], PhC cavities in semiconductor wires [24–26] or in 2D PhC membranes [27–29], see Fig. 1.

In general, the light confinement in cavities relying only on refraction is well understood as resulting from whispering-gallery modes. Our current understanding of the confinement in PhC cavities is much less mature, probably because the hybrid character of the confinement is conceptually difficult to apprehend. This difficulty is reflected in the design strategy that often relies on a global analysis of the cavity with 3D electromagnetic computations followed by optimisations performed by repeatedly adjusting some cavity parameters, see [30–36] for instance. For future applications and developments, it appears essential to deeply understand the confinement mechanisms in these cavities. A good understanding is also important for new designs in general.

Hereafter, we review the different physical mechanisms at work in the photon confinement of almost all modern PhC cavity constructs. For that purpose, we abandon the global analysis approach briefly summarized in Sect. 2 and we consider in Sect. 3 a classical description of the confinement through a Fabry-Perot picture. The latter emphasizes three intrinsic quantities (the mirror reflectance, the mirror penetration depth and the defect-mode group velocity), which are tightly attached to the physics of the electromagnetic confinement, but are hidden by global analysis. In Sect. 4, the main PhC cavity constructs that have a strong impact in the domain are dissected with the Fabry-Perot picture and the physical quantities that govern the performances are compared. From the comparison, general recipes for designing high-Q microcavities are discussed. Not all PhC microcavities can be accurately analysed with a few intrinsic quantities, and Sect. 5 is devoted to some subtle scattering mechanisms that may significantly alter the Fabry-Perot picture. As a whole, we expect that the overview helps to clarify the physical mechanisms and strategies that may be used for trapping light in subwavelength volumes.

2. Cavity Q-factors: definition and analysis

Resonant cavities have discrete frequencies of oscillation with a definite field configuration. This implies that, for an ideal lossless case, the response of the cavity to external excitation is a discrete set of infinitely narrow peaks, one for each eigenfrequency. In a real situation, appreciable excitation can occur for a narrow band around the resonance frequency. The source of this resonance broadening is energy dissipation. An important physical parameter that measures the sharpness of the resonator response is the quality factor Q. In the following, we will focus on dielectric microresonators, i.e. resonant structures with real permittivities and permeabilities. Hence, there is no absorption and the energy dissipation comes only from the power that leaks out of the cavity. The latter behaves as an open system.

Generally speaking, the quality factor Q of a resonator is defined as 2π times the ratio of the time-averaged energy stored in the cavity to the energy loss per cycle [37]:

$$Q = \omega_0 \frac{\text{Stored energy}}{\text{Power loss}} = \omega_0 \frac{U}{P} \,. \qquad (1)$$

In this definition based on an energy balance, U is the electromagnetic energy stored in the resonator and P is the power radiated out. Eq. (1) implies that the energy stored in the cavity is exponentially decaying in time with a decay time $\tau = Q/\omega_0$. The quality factor is therefore a measure of the cavity-mode lifetime. This intuitive and meaningful property is exploited by finite-difference-time-domain (FDTD) methods to compute cavity Qs [28, 31–33, 35].

It is relevant to consider also the frequency-domain definition of the Q factor and to show that the time-domain and the frequency-domain pictures are completely equivalent. In the frequency-domain picture, cavity modes and their associated Q factors are defined by considering analytical continuations of Maxwell's equations in the complex frequency plane. The cavity eigenmodes are defined as triplets $(\mathbf{E}, \mathbf{H}, \tilde{\omega})$ that are solutions of Maxwell's equations without sources

$$\nabla \times \mathbf{E} = i\tilde{\omega}\mu(\mathbf{r})\mathbf{H} \quad \text{and} \quad \nabla \times \mathbf{H} = -i\tilde{\omega}\varepsilon(\mathbf{r})\mathbf{E} \,, \quad (2)$$

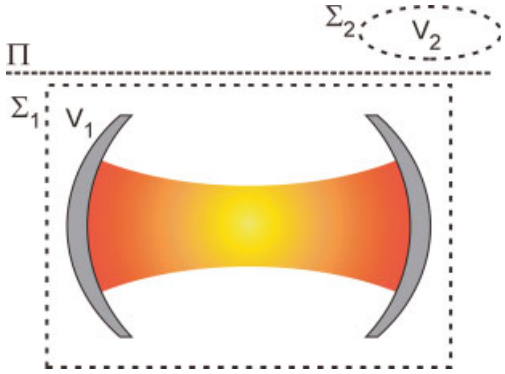

Figure 2 (online color at: www.lpr-journal.org) Schematic of the cavity mode of an optical open resonator. The two surfaces Σ_1 and Σ_2 can be used to define the quality factor Q.

where ε and μ are the real permittivity and permeability, respectively. For the sake of simplicity, we assume isotropic materials hereafter, but this assumption is not required. We will show now that the Q factor of the mode can be calculated from the imaginary part of the complex eigenfrequency $\tilde{\omega}$.

For that purpose, let us consider the triplet $(\mathbf{E}^*, -\mathbf{H}^*, \tilde{\omega}^*)$. By conjugating Eq. (2), it is shown that the triplet $(\mathbf{E}^*, -\mathbf{H}^*, \tilde{\omega}^*)$ is a solution of Maxwell's equations, since ε and μ are assumed to be real. Applying the Green-Ostrogradski formula to the vector $\mathbf{E} \times \mathbf{H}^* + \mathbf{E}^* \times \mathbf{H}$ on an arbitrary closed surface Σ defining a volume V, one obtains

$$\iint_{\Sigma} (\mathbf{E} \times \mathbf{H}^* + \mathbf{E}^* \times \mathbf{H}) \bullet d\mathbf{S} = i(\tilde{\omega} - \tilde{\omega}^*) \iiint_{V} (\varepsilon |\mathbf{E}|^2 + \mu |\mathbf{H}|^2) dV \,. \qquad (3)$$

Eq. (3) is a particular form of the Lorentz reciprocity theorem [38]. It is noteworthy that the closed surface used to derive Eq. (3) can be chosen arbitrarily. It may enclose the cavity (surface Σ_1 in Fig. 2) or may be located outside the resonator in the open space (surface Σ_2 in Fig. 2). By introducing the flux of the Poynting vector through the closed surface, $P = 1/2 \iint_{\Sigma} \mathrm{Re}(\mathbf{E} \times \mathbf{H}^*) \bullet d\mathbf{S}$, and the time-averaged electromagnetic energy stored in the volume $V, U = 1/4 \iiint_{V} (\varepsilon |\mathbf{E}|^2 + \mu |\mathbf{H}|^2) dV$, Eq. (3) can be rewritten as $P = -2\,\mathrm{Im}(\tilde{\omega}) U$, where P and U are defined for the cavity eigenmode. From Eq. (1), we infer that the Q factor is given by the ratio of the real part to the imaginary part of $\tilde{\omega}$,

$$Q = -\frac{\mathrm{Re}\,(\tilde{\omega})}{2\,\mathrm{Im}\,(\tilde{\omega})} \,. \qquad (4)$$

This relation shows that a damped oscillation at a real frequency ω_0 with a decay time $\tau = Q/\omega_0$ is equivalent to a lossless oscillation at a complex resonance frequency $\tilde{\omega} = \omega_0 - \mathrm{i}\omega_0/2Q$. Eq. (4) is often used by frequency-domain methods for calculating quality factors. Another usual approach that does not rely on analytical continuations consists of studying the frequency response of the resonator. For real excitation frequencies, the complex pole $\tilde{\omega}$ results in a Lorentzian-shaped resonance and the quality factor is given by $Q = \omega_0/\Delta\omega$, where $\Delta\omega$ is the full width at half-maximum.

Calculating cavity Q factors in the time domain with FDTD methods or in the frequency domain with frequency methods is fully equivalent in principle. The calculation basically consists of estimating global quantities such as the stored energy or the energy leaked per unit time. In general, it provides little physical insight into the nature of the confinement and little recipes for further designs. This is why the design of PhC microcavities with high Qs and small Vs has proved difficult from the beginning [39]. The usual approach is to start with a particular geometry that is known to confine light to some degree – such as a defect created by the absence of one or more adjacent holes in a photonic crystal – and then to repeatedly vary the parameters such as the size and location of the surrounding holes until the calculated Q reaches some large value.

In order to understand why some constructs perform better than others, several authors have introduced the concept of Fourier synthesis [32, 33]. The approach consists in calculating the Fourier transform of the cavity-mode electromagnetic fields in a plane, and then in looking for the Fourier components that lie within the light cone of the cladding materials. Provided that the Fourier spectrum analysis is performed in a plane above the cavity in the uniform air clad (such as the plane Π in Fig. 2), the Fourier components within the light cone correspond to propagative plane waves that leak out of the cavity. Therefore, their total contribution amounts to evaluate the Poynting vector flux P or the far-field radiation diagram of the cavity [32]. In the early 2000s, this approach has led to a breakthrough in the quest of cavity constructs with high Q factors [28]. It was found that the cavity-mode electric field should decay slowly in the mirrors to suppress out-of-slab photon leakage.

But although successful, this approach relies on an a posteriori analysis of a global property of the cavity mode and, since it is not intuitively clear how to relate a given mode profile to a given cavity geometry without computing the cavity mode itself, the Fourier analysis does not remove much of the guess work for the cavity designer. In addition, even if one may find an approximate analytical relation [35] between a given field profile and the cavity geometry that would support the profile, the global analysis approaches do not identify the few important physical quantities that govern the light confinement. For many interesting cavity constructs, this can be remedied by analyzing the photon confinement with a Fabry-Perot model. The latter as will be discussed in the next section, represents a mesoscopic confinement description, which relies on intrinsic physical parameters (mirror reflectance, modal properties of the trapped mode . . .) rather than on global properties of the cavity mode (lifetime, far-field radiation diagram . . .).

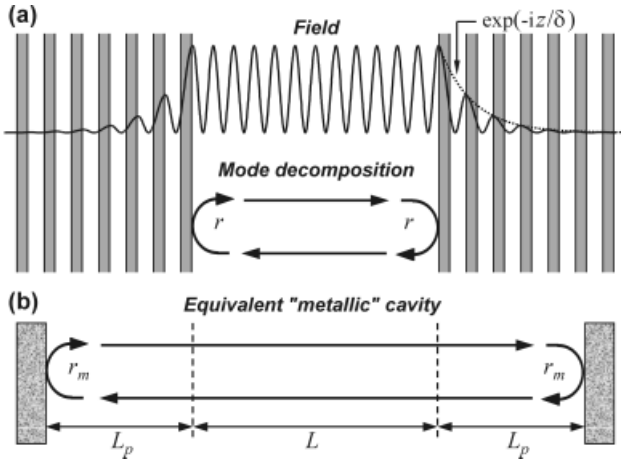

Figure 3 Fabry-Perot resonator with distributed mirrors. (a) Electric field of the cavity mode. (b) Equivalent "metallic" cavity. The defect mode is now cycling over a larger effective cavity length $L_{\text{eff}} = L + 2L_p$ between two mirrors with a metallic-like reflection coefficient r_m independent of the wavelength. The cavities in (a) and (b) have the same resonance frequency and the same Q factor, but their mode volumes are obviously different.

3. Fabry-Perot model of photonic crystal cavities

3.1. Fabry-Perot model

Interpreting the light confinement in a resonator with a Fabry-Perot model consists in approximating the cavity mode as a stationary pattern formed by two counter-propagating defect modes bouncing between two mirrors, see Fig. 3. In a- and b-type resonators (Fig. 1), the defect mode is the fundamental guided mode of a z-invariant waveguide. In a c-type resonator, it is the gap-guided Bloch mode of a z-periodic waveguide, a single-row-defect PhC waveguide for the example shown in Fig. 1. These modes all obey a dispersion relation $\omega(k_z)$, and are thus characterized by an effective index $n_{\text{eff}} = k_z/k_0$ and by a group index $n_g = c(d\omega/dk_z)^{-1}$. For classical z-invariant waveguides like in a- or b-type microcavities, n_{eff} and n_g only slightly differ, but for c-type microcavities, the waveguide potentially supports slow Bloch modes and confinement regimes with slow photons ($n_g \gg n_{\text{eff}}$) trapped between two mirrors may be observed. The dispersion relation of the defect mode is therefore an important quantity of the Fabry-Perot model.

Another important quantity is the modal reflection coefficient $r = |r|\exp(i\phi)$ of the mirror. When the defect-guided mode impinges onto the mirror, it is backreflected into the counter-propagating guided mode, which is again backreflected onto the second mirror. Under the assumption (this assumption will be always valid in the following) that the bouncing mode is truly guided, no radiation loss occurs when light propagates from one mirror to the other one. As a consequence, the cavity-mode lifetime is only limited by the imperfect mirror reflectivity, $R = |r|^2$, a quantity strictly smaller than 1 for propagative modes. Light can be either transmitted into an output waveguide (often a desired effect for coupling into another channel), or radiated out into the cladding (in general a detrimental effect). The origin of these radiation losses is the termination experienced by the incident guided mode at the waveguide/mirror interface [40].

Within the Fabry-Perot picture, a resonance at a wavelength $\lambda_0 (k_0 = 2\pi/\lambda_0)$ results from a phase-matching condition for the defect mode. The total phase delay $\Phi_T(\lambda_0)$ experienced by the guided mode along one-half cavity cycle has to be equal to a multiple of π [41],

$$\Phi_T(\lambda_0) = k_0 n_{\text{eff}} L + \phi(\lambda_0) = p\pi\,, \tag{5}$$

where L is the physical cavity length (side-to-side separation distance between the two mirrors, see Fig. 3) and p is an integer. For narrow resonances ($\Delta\lambda \ll \lambda_0$), the Q factor can be straightforwardly expressed as the derivative of $\Phi_T(\lambda)$ and, after neglecting the dependence of $|r|$ with the wavelength, one obtains

$$Q = \frac{\pi}{1-R}\left[\frac{2Ln_{\text{g}}}{\lambda_0} - \frac{\lambda_0}{\pi}\left(\frac{\partial\phi}{\partial\lambda}\right)_{\lambda_0}\right]. \tag{6}$$

It is relevant to introduce the penetration length into the distributed mirrors, $L_p = -\lambda_0^2/(4\pi n_g)(\frac{\partial\phi}{\partial\lambda})_{\lambda_0}$ shown in Fig. 3, so that Eq. (6) is simply rewritten

$$Q = \frac{k_0}{1-R} n_{\text{g}}(L + 2L_{\text{p}})\,. \tag{7}$$

The quantity $L_{\text{eff}} = L + 2L_p$ that is often called the effective cavity length has a simple analogy. It represents the physical length of an equivalent cavity formed by two metallic mirrors. The cavity with PhC mirrors is analogous to a cavity formed by the bouncing of the same waveguide mode between two metallic mirrors separated by a distance L_{eff}. In particular, both cavities possess the same resonance wavelength, given by Eq. (5), and the same Q factor, given by Eq. (7), provided that the metallic reflectors possess a reflection coefficient r_m independent of the wavelength and equal to $r_m = |r|\exp[i(\phi - 2k_0 n_{\text{eff}} L_p)]$.

According to Eq. (7), only three physically meaningful quantities govern the Q factor, namely the group index n_g of the trapped mode, the effective length L_{eff} and the modal reflectivity R. As will be shown in Sect. 4, all these quantities significantly impact the performance of PhC cavities.

3.2. Validation of the Fabry-Perot model

PhC cavities exhibit various appearances and, a priori, it is not obvious to predict whether a specific construct behaves as a simple Fabry-Perot resonator or not. According to the classification table of the review article by Vahala [6],

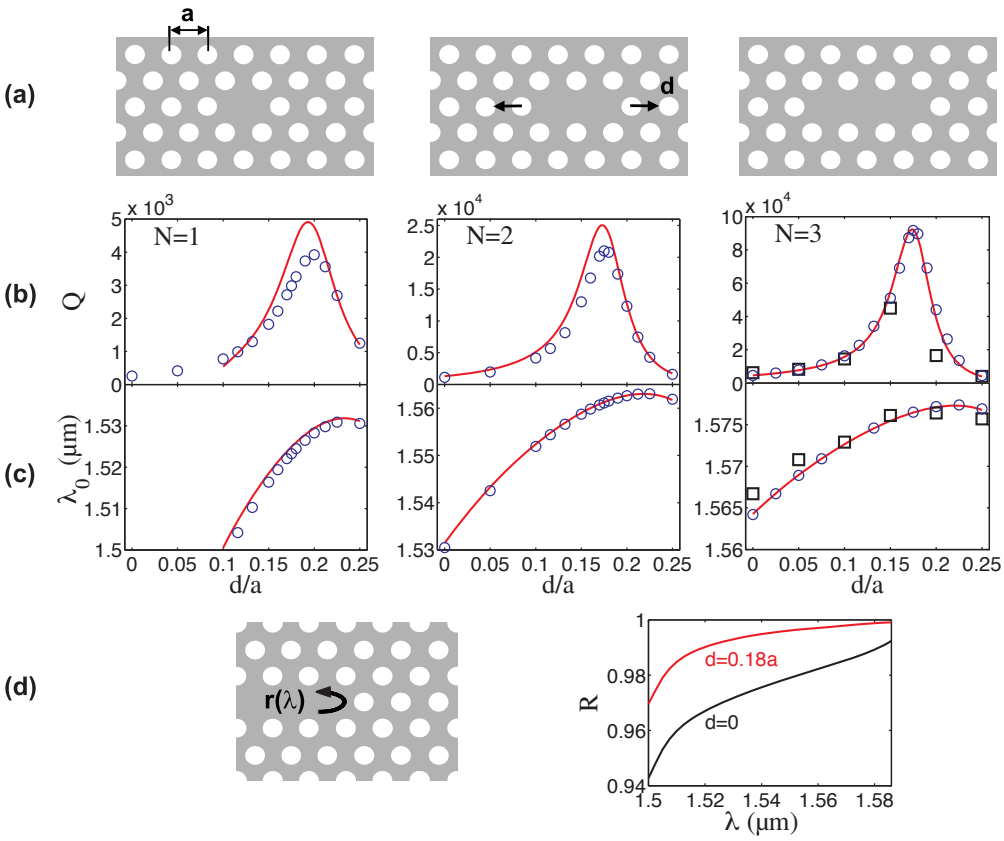

Figure 4 (online color at: www.lpr-journal.org) Validation of the Fabry-Perot model for nanocavities in a two-dimensional PhC membrane. (a) Sketch of L1, L2 and L3 cavities with $N = 1$, 2, and 3 missing holes. (b) and (c) Comparison between fully vectorial calculation data (blue circles) and Fabry-Perot model predictions (red solid curves) for the cavity Q and for the resonance wavelength λ_0 as a function of the normalized hole displacement d/a. The experimental data obtained in [28] are shown with squares for $N = 3$. (d) Two examples of mirror reflectivity spectra $R = |r(\lambda)|^2$ used in the Fabry-Perot model to compute the red curves in (b).

only a- and b-type resonators (see Fig. 1) would behave as Fabry-Perot resonators, whereas the confinement method for c-type cavities in 2D PhC membranes is understood as resulting from a different mechanism and deserves a specific column in the table. This classification relies on geometrical considerations rather than on an in-depth analysis of the confinement mechanisms and it is somewhat arbitrary in our opinion. Indeed, as will be shown in Sect. 5, light confinements in micropillars do not follow a classical Fabry-Perot description, whereas, as will be shown now, many important c-type cavities in 2D PhC membranes behave as classical Fabry-Perot resonators.

To illustrate our purpose, let us consider three PhC cavities obtained by removing $N = 1$, 2, and 3 holes in a 2D PhC slab, see Fig. 4a for a schematic view of the cavities along with a definition of the main parameters. Figs. 4b and 4c show the Q factor and the resonance wavelength λ_0 as a function of the displacement d of the two inner cavity holes. The blue circles are obtained by computing the resonator complex pole $\tilde{\omega}$ with a fully vectorial aperiodic-Fourier modal method (a-FMM) [42]. For the sake of comparison, we also include experimental data (squares) obtained for the cavity with $N = 3$ [28]. In Figs. 4b and 4c, the solid red curves are Fabry-Perot model predictions for Q and λ_0 obtained from Eqs. (5) and (7). The predictions rely on the sole knowledge of the dispersion curve of the single-row-defect waveguide and on the mirror modal reflection $r(\lambda)$ computed with a generalized version of the a-FMM [43] to analytically handle light propagation in z-periodic waveguide stacks. The mirror modal reflectivity $R = |r|^2$ is shown in Fig. 4d for two particular hole displacements, $d = 0$ and $d = 0.18a$. The net effect of the tiny hole shift by $0.18a$ is an increase of the mirror reflectivity over the entire spectral range of interest. The reason for this effect is analyzed in the next section.

The quantitative agreement between the Fabry-Perot model predictions (solid red curves) and the experimental (squares) and numerical (circles) data suggests that light confinement in 2D PhC slab microcavities can be largely understood as a Fabry-Perot mode formed by the bouncing of the fundamental mode of the single-row-defect PhC waveguide, and this even for ultrasmall cavities with a single hole missing ($N = 1$). Compared to the global approaches discussed in Sect. 2, the Fabry-Perot model clearly provides a conceptually helpful picture, since analyzing a mirror is much simpler than analyzing a whole cavity. It additionally provides new hints for improving cavity performance, such as engineering the mirror/waveguide interface to lower the radiation losses or slowing down the group velocity of the trapped mode.

However, some PhC microcavities do not behave as Fabry-Perot resonators. But even when the Fabry-Perot model fails at predicting the performance of a specific construct, it is important to be aware of that and to analyze why. The understanding gained may then provide new routes or recipes for further improvements, see Sect. 5.

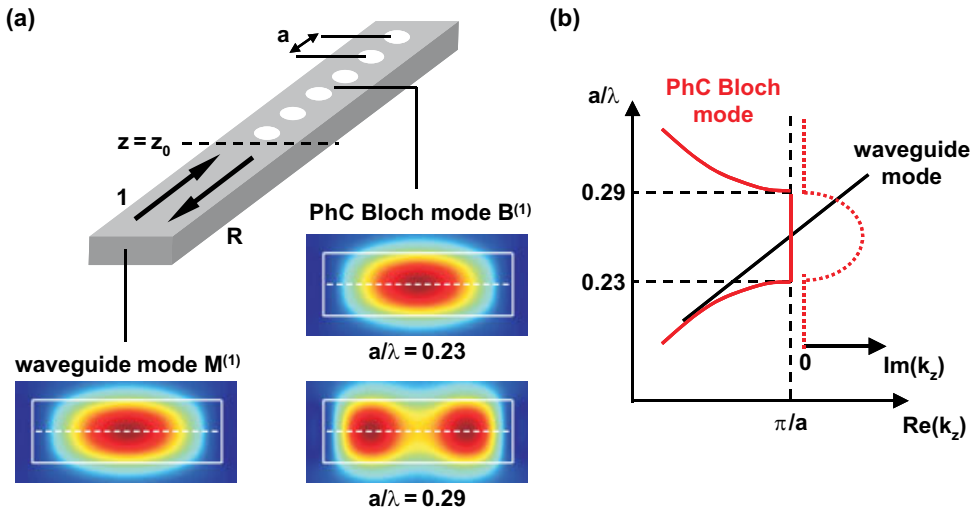

Figure 5 (online color at: www.lpr-journal.org) Transverse mode-profile mismatch at a waveguide/mirror interface. (a) Cross-sectional profiles of the fundamental modes $\mathbf{M}^{(1)}$ and $\mathbf{B}^{(1)}$ of a z-invariant air-bridge waveguide (left) and of the associated PhC mirror Bloch mode (right). (b) Dispersion diagram of the two fundamental modes supported by the waveguide ($\mathbf{M}^{(1)}$ shown with a black curve) and by the mirror ($\mathbf{B}^{(1)}$ shown with a solid red curve). In the gap, the mirror Bloch mode $\mathbf{B}^{(1)}$ is guided but purely evanescent ($k_z = \pi/a + i\,\mathrm{Im}(k_z)$). The computations are performed with the a-FMM for a 340-nm thick, 500-nm wide silicon air-bridge, for a mirror periodicity $a = 420$ nm and for a hole diameter of 230 nm.

4. Recipes for high-Q Fabry-Perot resonators

As general design recipes, the Fabry-Perot model suggests that three physical quantities may impact the design of high-Q microcavities, namely the modal reflectivity R, the group index n_g of the defect mode and the effective cavity length $L + 2L_p$. Indeed, the most important quantity is the modal reflectivity R. Recipes for increasing R are summarized in Sect. 4.1. Sect. 4.2 discusses cavities formed by trapping a slow mode between two mirrors. Although it has been shown to impact the mode lifetime of important PhC microcavities [44, 45], slowing down the speed of the trapped (defect) mode to boost the Q factor has not received much attention in the literature. The cavity Q factor can be simply increased by using a larger physical defect length, but this is immediately compensated by an increase of the mode volume, so that the ratio Q/V is kept unchanged. As detailed in Sect. 4.3, the impact on Q and V of the penetration depth L_p is not as intuitively clear and deserves more attention.

4.1. Mode matching at the mirror/defect interface

Before considering recipes for designing mirrors offering large reflectivities close to unity, let us first consider light reflection at an abrupt interface between a monomode wire and a semi-infinite PhC mirror, see Fig. 5a. The total electromagnetic field in the z-invariant waveguide, $\mathbf{\Phi} = |\mathbf{E}, \mathbf{H}\rangle$, can be expanded in terms of the complete set of normal modes. Let us denote by $\mathbf{M}^{(1)}$ the incident fundamental mode of the waveguide and by $\mathbf{M}^{(-1)}$ the associated backward propagating mode. For $z < z_0$, see Fig. 5a for a definition of z_0, we have

$$\mathbf{\Phi} = \mathbf{M}^{(1)} + r\mathbf{M}^{(-1)} + \sum_{p>1} r^{(p)}\mathbf{M}^{(-p)}\,, \qquad (8)$$

where $\mathbf{M}^{(-p)}, p > 1$, are the backward-propagating radiation modes and the $r^{(p)}$ are the modal reflection coefficients of the backward-propagating modes. Similarly, in the mirror, only the forward-propagating Bloch modes $\mathbf{B}^{(p)}, p > 0$, are excited, and the total field can be written for $z > z_0$,

$$\mathbf{\Phi} = t\mathbf{B}^{(1)} + \sum_{p>1} t^{(p)}\mathbf{B}^{(p)}\,, \qquad (9)$$

where $t^{(p)}$ are the modal transmission coefficients of the forward-propagating Bloch modes. In Eq. (9), a specific Bloch mode $\mathbf{B}^{(1)}$ has been isolated from the summation. In the perturbation regime with infinitely small holes, the mirror Bloch modes should be similar to the modes of the z-invariant waveguide, and one may associate a Bloch mode $\mathbf{B}^{(p)}$ of the mirror to every mode $\mathbf{M}^{(p)}$ (guided or radiative) of the z-invariant waveguide. $\mathbf{B}^{(1)}$ is simply defined as the Bloch mode associated to $\mathbf{M}^{(1)}$. Even for infinitely small holes, a bandgap is opened in the dispersion relation of the periodic waveguide. Thus, the Bloch mode $\mathbf{B}^{(1)}$, which is truly guided at low frequencies, is either a propagative mode ($\mathrm{Im}(k_z) = 0$) outside the bandgap, or a purely evanescent mode ($k_z = \pi/a + i\,\mathrm{Im}(k_z)$) inside the bandgap. Fig. 5b shows the dispersion diagrams of $\mathbf{M}^{(1)}$

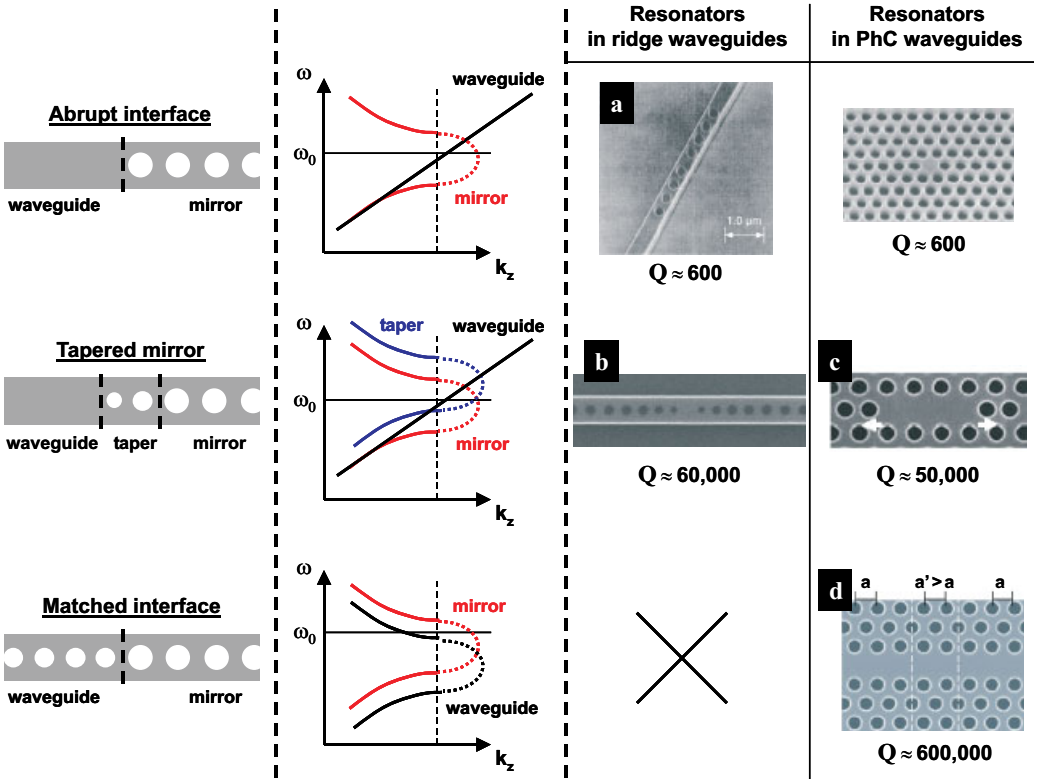

Figure 6 (online color at: www.lpr-journal.org) Strategies for designing high-Q Fabry-Perot resonators. Upper row: the Q factors of cavities with abrupt interfaces are limited to a few hundreds. Second row: cavities with tapered mirrors. Third row: matched interface relying on a small mismatch between the waveguide mode and the mirror Bloch mode. a. PhC cavity in ridge waveguides, after [25] b. Id, after [55] c. L3 cavity, after [28] d. Heterostructure cavity, after [59].

(black curve) and $\mathbf{B}^{(1)}$ (solid red curve). Note that the dotted red curve inside the bandgap represents the imaginary part $\mathrm{Im}(k_z)$ of the Bloch-mode propagation constant.

The stationary Bloch mode $\mathbf{B}^{(1)}$ plays a central role in the backreflection process, since its excitation is responsible for the reflection of the incident mode. Because the Bloch mode penetrates into the low-index material (the hole), the transverse mode profiles of $\mathbf{M}^{(1)}$ and $\mathbf{B}^{(1)}$ are different. The mismatch [40] is responsible for the excitation of Bloch modes $\mathbf{B}^{(p)}$ other than $\mathbf{B}^{(1)}$ at the abrupt interface, and inevitably some light leaks out in the cladding ($R < 1$). As shown in Fig. 5a, the transverse mode profile of $\mathbf{B}^{(1)}$ strongly depends on the operation frequency, or for a fixed frequency on the mirror period a. The latter thus represents an important degree of freedom for engineering tapers that progressively reduce the transverse mode profile mismatch as light penetrates into them [40, 46–48].

From the previous analysis, one clearly realizes that it is critical to engineer the interface between the waveguide and the mirror in order to lower the mismatch. Fig. 6 summarizes the general strategies adopted so far. The first small-V cavities in semiconductor wafers have been fabricated mainly for laser applications in planar waveguides with PhC mirrors composed of slits and ridges [49–51], and then in wire waveguides with PhC mirrors composed of hole chains [24, 25]. For abrupt interfaces between the waveguide and the mirror (first row in Fig. 6), the mismatch results in a few per cent losses at the gap-center frequency, and the cavity Qs do not exceed several hundreds.

Lowering the mismatch may be achieved by engineering the interface between the waveguide and the mirror to implement tapered mirrors [40, 46]. The single-hole-displacement approach discussed in Fig. 4d is an illustrative example [44, 45]. Nowadays, efficient tapers (second row in Fig. 6) are designed in a systematic way by using a progressive variation of the geometric parameters. They are composed of a series of intermediate sections, which support Bloch modes that implement a gradual Bloch-mode-profile variation from $\mathbf{M}^{(1)}$ to $\mathbf{B}^{(1)}$ [46, 47]. The first attempt to fabricate cavities with tapered mirrors was performed for ridges with Bragg mirrors composed of slits [52], but the experimental evidence of the beneficial effect of the taper has been plugged by mode mixing in the multimode ridge, as evidenced by further near-field measurements of the cavity mode [53]. The most sophisticated tapers [26, 54–57] currently involve three to four sections and provide a very gradual profile variation. It is crucial to implement the taper between the mirror and the defect waveguide, since at resonance photons experience many times the transition before escaping the cavity, but it is also important to

	Q (exp.)	R (exp.)	n_g	L_{eff} (μm)	$V(\lambda^3)$
Ridge PhC cavity [55]	60 000	0.9996	4	1.2	0.014
L3 cavity [28]	45 000	0.997	13	2.6	0.019
Heterostructure cavity [59]	600 000	0.9993	16	6.7	0.028

Table 1 Physical parameters of representative high-Q PhC cavities.

taper photons out of the cavity for the sake of absolute transmission enhancement [56]. When associated to form a cavity, these tapered mirrors provide typical experimental Q values in the range of 10 000–200 000 for single-defect resonators in semiconductor ridges on silicon-on-insulator substrates [26, 54–57] or in PhC waveguides in various semiconductor membranes in air [58]. In general, the taper is designed by purely numerical optimisation techniques, but hand-driven designs relying on evanescent Bloch-mode engineering have also been proven successful [26, 46, 47]. The modal reflectivity of tapered mirrors varies between 0.997 for the L3 cavity to 0.9996 for cavities in ridge waveguides, see Table 1.

Another strategy that has recently resulted in a milestone improvement is based on single-row-defect PhC cavities with "naturally" matched interfaces (third row in Fig. 6). In the so-called heterostructure nanocavity [59], the waveguide and mirror geometries are very similar. Even without engineering the interface, the mirror performance is remarkable ($R = 0.9993$), see Table 1. Further engineering of the interface by tapering leads to experimental Q values in the excess of 10^6 with theoretical predictions greater than 10^7 [59–61].

4.2. The group-velocity effect

For classical Fabry-Perot resonators in z-invariant waveguides like micropillars or PhC cavities in ridge waveguides, the defect-guided mode possesses group and phase velocities that are essentially comparable. The situation is radically different for microcavities in 2D PhC membranes. The defect becomes a periodic waveguide that may support a slow mode. Potentially, if the frequencies of the slow mode and of the cavity mode are matched, not only is the light trapped between the mirrors as in a classical Fabry-Perot resonator, but it also travels slowly from one mirror to the other, still increasing the cavity lifetime by a factor proportional to the group index of the defect mode. Table 1 shows the group indices of the defect mode for various PhC cavities. For cavities in ridge waveguides, the group index ($n_g = 4$) is nearly equal to the refractive index of the host material and no slowdown effect is expected. The situation is different for microcavities in PhC waveguides, like the L3 ($n_g = 13$) and the heterostructure ($n_g = 16$) cavities, for which the slowdown effect results in a 3- to 4-fold Q factor enhancement.

Boosting the Q factor of PhC cavities by trapping slow waves has been first proposed in [44, 45], in order to interpret part of the surprising experimental observation of the Q-factor enhancement in the L3 cavity by slightly shifting the two inner holes, see Fig. 4. Although intuitively clear, this strategy has not been much considered in the literature as a recipe for designing high-Q microcavities. For in-line geometries, designs exist for $n_g = 25$ but they have not been tested experimentally [45, 62]. The concept has been recently extended to 2D Bloch modes by considering slow Bloch modes at the band edges of a 2D PhC slab. In these entirely new constructs that abandon the in-line geometry, the 2D Bloch mode may operate below the light line of the cladding material offering ultrahigh Q values [63] or above the light line with moderate Q values ($Q \approx 40\,000$), but with a highly directional out-of-plane radiation pattern that may be useful for active device applications like vertical-emission lasers [64].

4.3. Comparison of various PhC cavities

Table 1 summarizes our discussion and describes the main lessons learned by applying a Fabry-Perot model to interpret light confinement in modern PhC microcavity constructs. The experimental Q and calculated V data are both taken from the related publications. For every cavity, we have calculated the group index n_g of the defect mode for the resonance wavelength λ_0 and for the geometrical parameters (hole diameter, hole separation distances…) deduced from MEB observations of the actual samples. We have also calculated the modal reflection coefficient $r = |r| \exp(i\phi)$ of the PhC mirrors by using a fully vectorial modal method [43]. The reflectivity $R = |r|^2$ depends on the in-plane coupling of loaded cavities. Additionally, it is likely to be sensitive to fabrication errors such as the inevitable surface roughness or the actual deviation of the hole sizes from one hole to the other. However, as we checked numerically, the penetration depth L_p that is essentially given by $(\partial\phi/\partial\lambda)$ weakly depends on the fabrication errors and on the loading, hence the effective cavity length $L_{\text{eff}} = L + 2L_p$ can be reliably estimated numerically. We have then extracted the modal reflectivity R (third column) from the experimental values of the Q factor by applying Eq. (7). Thus, the R data can be considered as experimentally inferred reflectivities that take into account fabrication errors and loading effects.

As shown by the table, state-of-the-art PhC microcavities all possess a remarkably high modal reflectivity, close to 0.999. This corresponds to two additional nine digits in comparison with the first photonic bandgap microcavity ($R = 0.96$ for the cavity in Fig. 6a) fabricated in the late 1990s [25]. However, it is worth mentioning that state-of-the-art reflectivities for dielectric Bragg mirrors with up-to-date automated deposition techniques are still much

larger [65]. In addition, we note that one is currently concerned with controlling uniformity and roughness on 10-cm^2 scales in thin films coatings, whereas the PhC reflectors are concerned with guided modes with μm^2 cross sections. It is also noteworthy that the microcavities in PhC waveguides take benefit from a slowdown effect that boosts the cavity Q factor by a factor 3 to 4 in comparison to cavities in classical z-invariant ridge waveguides.

Clearly, increasing the physical cavity length L of the cavity is of no help, since V and Q both scale linearly with L(Q/V remains unchanged). Note that similar conclusions do not hold if the objective is to enhance nonlinear phenomena since the operation powers do not generally scale as Q/V. The impact of the penetration depth L_p on Q/V is subtler. As we learn from classical textbooks [66], the penetration depth of classical quarter-wave Bragg mirrors is related to the number of dielectric pairs required for efficient reflection. Thus, one could naively expect that the mode volume scales linearly with L_p and that an increase of L_p is also not beneficial. This is actually not true, simply because the mode volume is not related to L_p in general, but rather to the decay length δ of the electromagnetic field in the mirror, see Fig. 3. This length is given by the imaginary part $\mathrm{Im}(k_z)$ of the predominant mirror Bloch mode $\mathbf{B}^{(1)}$. Only for classical Bragg mirrors used at the Bragg wavelengths, are L_p and δ related. In Table 1, it is interesting to note that the heterostructure cavity possesses the highest L_{eff} value. The latter is five times larger than that of the ridge PhC cavity and is more than two times larger than that of the L3 cavity. In comparison, the associated mode-volume increase is rather modest. As discussed in the supplementary information of [59], the increase of the mode volume remains small because the decay length of the mirror Bloch mode is abnormally small for such an operating wavelength in the close vicinity of the band edge.

5. Beyond the Fabry-Perot model of photon confinement

Although the use of a Fabry-Perot model is clearly the prime approach for analysing the physics of photon confinement in cavities, not all microcavities are expected to behave perfectly as Fabry-Perot resonators. As illustrated in Fig. 4, small deviations of the Q factor and of the resonance wavelength are obtained for $N = 1$ and $N = 2$. The reason is that in the Fabry-Perot picture, the energy transport between the two mirrors is assumed to be solely ensured by the fundamental propagating mode $\mathbf{M}^{(1)}$ of the defect waveguide, with all other energy-transport routes being neglected. These other routes are the modes $\mathbf{M}^{(p)}, p \neq 1$. Two study cases may be considered depending on the existence of guided modes other than the fundamental one in the defect waveguide.

For monomode waveguides as in Fig. 4, the other modes $\mathbf{M}^{(p)}, p \neq 1$, are all radiative. They leak out of the waveguide and their leakage guarantees that their impact on the cavity-mode lifetime vanishes as the defect length increases. This trend is clearly observed in Fig. 4. Although kept at a negligible level for the L1–L3 cavities, the impact of the leaky modes on ultrasmall resonators can be very important for globally optimised structures. For instance, PhC cavities optimized by finely tuning the position and the diameter of the two inner holes of the mirrors in a ridge waveguide may offer Q values as high as 10^5, although the mirror performance is kept at a modest level, $R < 0.99$. This counterintuitive effect has been interpreted as a recycling of a substantial fraction of the mirror radiation losses by leaky waves that are excited at the defect/mirror interfaces and that contribute to efficiently transfer energy between the two mirrors [34]. The recycling effect has been observed from transmission measurements performed for cavities formed in planar waveguides with mirrors composed of ridges and grooves [67] or with mirrors composed of holes [68], and Q values in excess of those predicted by a Fabry-Perot model have been effectively measured. Similar phenomena are probably encountered in many PhC cavity constructs that are designed through a global strategy by repetitively varying the locations and the diameters of the nearest-neighbor holes to optimize the cavity Q. In general, for subwavelength defect lengths, the optimization process is successful and recycling and tapering processes join together to achieve large enhancements of the Q factor. Although full assessment would require that the mirror reflectance be calculated, the single-hole-defect cavities in [17, 32, 69] are likely to combine these two effects.

The second study case concerns cavities for which the defect waveguide supports several truly guided modes. This situation is classically encountered for GaAs/AlGaAs pillar microcavities. The latter have played a major role in the development of several optoelectronic devices, including vertical cavity-surface emitting lasers [21], and in the realization of the first cavity quantum electrodynamic experiments in the solid state [7, 8, 70–73]. Naively, one could imagine that those in-line small-index-contrast III-V cavities represent archetypal Fabry-Perot resonators. For large diameters ($d > \lambda_0$), this is actually true and photoluminescence experiments reveal a series of resonances that is easily associated to the different trapped propagating defect modes $\mathbf{M}^{(p)}, p = 1, 2 \ldots$ The cavity modes can be seen as $\mathbf{M}^{(p)}$–$\mathbf{B}^{(p)}$ pairs that are all independent and the mode lifetimes are basically limited by the transmission through the top and bottom mirrors. For these cavities with large diameters, the photon confinement almost behaves as in the reference planar cavity and, although the spacer defect supports several propagating modes, the Fabry-Perot model actually applies and Q values in excess of 10^5 [22] can be achieved for mirrors with a large number of pairs.

The situation is radically different for smaller diameters, $\lambda_0/2 < d < \lambda_0$ [72]. What is happening is that the transverse mode-profile mismatch between the spacer modes $\mathbf{M}^{(p)}$ and their associated mirror Bloch modes $\mathbf{B}^{(p)}$ is increased by the lateral confinement. Thus, the propagating spacer modes $\mathbf{M}^{(p)}$ not only excite their associated Bloch

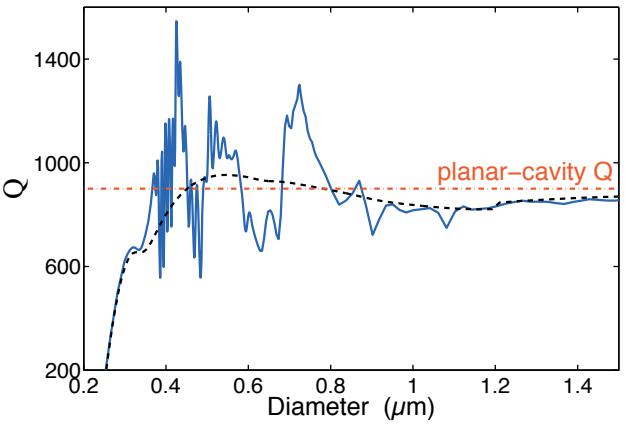

Figure 7 (online color at: www.lpr-journal.org) GaAs/GaAlAs micropillar Q factor as a function of the pillar diameter ($\lambda_0 = 0.95\,\mu$m). The solid blue curve represents fully vectorial computational results for top and bottom Bragg mirrors composed of 9 and 25 alternate layer periods, respectively. This corresponds to a planar-cavity Q of 900. The dashed black curve represent the Fabry-Perot model predictions obtained by considering that the pillar cavity mode is formed by the association of the $\mathbf{M}^{(1)}-\mathbf{B}^{(1)}$ pair only. More details of this surprising behavior can be found in [72, 74].

modes $\mathbf{B}^{(p)}$, but also other Bloch modes. The series of independent resonances is again observed in experiments, but each individual resonance can no longer be viewed as the associations of individual $\mathbf{M}^{(p)}-\mathbf{B}^{(p)}$ pairs, as for large diameters. In fact, the pairs couple together, and although every pillar eigenmode is dominated by the cycling of a predominant single $\mathbf{M}^{(p)}$ mode, it is slightly altered by the excitation of other defect and mirror modes. The Fabry-Perot picture no longer holds and the coupling results in an intricate oscillatory behavior of the Q factor as a function of the pillar diameters, see Fig. 7. For some diameter ranges, the Qfactors can reach values well in excess of the Q factor of the reference planar cavity. This may appear surprising [73], since one rather expects that the micropillar Qs is always smaller than that of the reference planar cavity obtained before etching, because etching offers an additional loss route, namely radiation into the air clad. But this argument is too simplistic. The fact that Q factors in excess of the planar cavity Q can be obtained at small diameters is fully understood in the mode-coupling description, see [74] for details, and has been recently observed by measuring the photoluminescence of InAs self-assembled quantum dots grown in the middle of the GaAs defects in a series of micropillars fabricated with diameters varying from 550 nm to 1.3 μm [23].

Clearly, the Fabry-Perot model is not a panacea and it may fail even for apparently simple in-line geometries. However, we have no doubt that, even for these particular cases, the Fabry-Perot model already represents a good first-order approximation that is useful for further engineering and optimization.

6. Conclusions

In the past decade, the performance of all types of PhC nanocavities has seen considerable progress. This clearly results from fabrication and material improvements, but design is also crucial. It is noteworthy that the Q-factor enhancements have been systematically accompanied by an increase of the mirror reflectivity through mode-matching strategies. The group velocity of the trapped-defect mode, which is often completely hidden in brute-force global computational analysis, is another important physical quantity that impacts the performance of state-of-the-art nanocavities.

Presently, nanocavities in 2D PhC membranes suspended in air combine mode volumes close to the theoretical limit $(\lambda/2n)^3$ and Q factors that are ten times larger than those achieved with other PhC geometries, like micropillars or nanocavities in ridge waveguides on a substrate. One may suspect that ultrahigh Qs are easier to achieve with 2D bandgap confinements, rather than with more traditional approaches based on 1D bandgap confinements. This is unclear in our opinion. First, one has to consider that 2D PhC cavities have been supported by a drastic research effort over the past few years. Additionally, one has to call that large mode lifetimes are much more difficult to achieve in constructs implemented on a substrate than in membranes suspended in air [26].

The realization of still higher Q factors will be challenging because fabricating mirrors with very small radiation losses in the range of 10^{-4} requires an accurate control of the hole positions and diameters in the nanometer range. However, there might be no real need to achieve such high Q factors in the future, and it is already important to realize all the benefits that may be taken from the present performance for future electrically driven devices [17] or optical nonlinearities [75].

Although often qualified as ultrasmall cavities, the typical mode volume of present PhC resonators is of the order of a few hundredths of λ^3. This volume is close to the theoretical limit, but it is still several orders of magnitude larger than the volume of nano-objects like molecules or quantum dots. Thus, despite the very high Q factors, there is a waste of space in the interaction reinforcement. New types of constructs that would remove this deficiency, while maintaining a high Q, have to be designed, and in this context, resonators relying on strong electric-field discontinuities in slot waveguides [76] or on localized plasmon resonances in metallo-dielectric particles [77] appear as interesting new departures. New design strategies allowing the realization of cavities that are only weakly sensitive to various types of disorders (roughness, hole diameter errors . . .) are likely to be highly desirable too [78]. Such immunity would considerably enhance the device yield.

Acknowledgements The authors acknowledge many interesting and stimulating discussions with their collaborators Guillaume Lecamp, Philippe Velha, Jean-Claude Rodier, David Peyrade,

Emmanuel Picard, Emmanuel Hadji, Isabelle Robert-Philip and Jean-Michel Gérard. They acknowledge supports from the MIRAMAN project PNANO06-0215, the NanoEPR project of the 2006 NanoSci-ERA programme and from the European contract SPLASH of the 6th EU Framework programme.

Philippe Lalanne is Ancien Elève of the Ecole Normale Supérieure de Saint Cloud. He received the Agrégation de Sciences Physiques and the M.S. degree in Solid State Physics in 1986, the PhD degree in Physics in 1989 and the Habilitation à diriger les recherches in 1996 from the University of Orsay. After his first-year researches in the field of Optical Information Processing, he spent a sabbatical year at the Institute of Optics, Rochester in 1995. Since then, he has been involved in computational physics and in applications of subwavelength optical structures for diffractive optics, plasmonics, photonic crystals, integrated optics and microcavities. He is presently Directeur de Recherche au CNRS. He received the Bronze Medal of CNRS (1993) and was awarded the Fabry de Gramont price from the Société Française d'Optique (1998). He is a member of the European Optical Society, the Optical Society of America, the IEEE LEOS and is a Fellow of the Institute of Physics and of the Optical Society of America.

Christophe Sauvan, born in 1978, received his M.S. degree in applied physics from the Ecole Centrale Paris in 2001 and completed his Ph.D. in optics and photonics from the Université Paris Sud in 2005. He was a postdoctoral research associate at the Laboratoire de Photonique de Nanostructures in 2006. He joined the Institut d'Optique in 2007 as a Chargé de Recherche CNRS. His current research interests include plasmonics, photonic crystals and microcavities.

Jean-Paul Hugonin is Ancien Elève of the Ecole Normale Supérieure de Saint Cloud. He received the Agrégation de Mathématique in 1974 and the M.S. degree in Optics in 1975, the Doctorat d'Etat ès Sciences degree in Physics in 1983 from the University of Orsay. He is now Maître de Conférence at the University of Paris VI. His current research interests concern computational physics and electromagnetism for various applications in image processing, diffractive optics, plasmonics, photonic crystals, integrated optics and microcavities.

References

[1] A. J. Shields, Semiconductor quantum light sources, Nature Photonics **1**, 215–223 (2007).
[2] H. M. Gibbs, Optical Bistability: Controlling Light with Light (Academic Press Orlando, FL, 1985)
[3] H. Yokoyama and K. Ujihara, Spontaneous Emission and Laser Oscillation in Microcavities (CRC Press, Florida, USA, 1995).
[4] T. J. Kippenberg and K. J. Vahala, Cavity opto-mechanics, Opt. Express **15**, 17172–17205 (2007).
[5] E. M. Purcell, Spontaneous emission probabilities at radio frequencies, Phys. Rev. **69**, 681 (1946).
[6] K. J. Vahala, Optical Microcavities, Nature **424**, 839–846 (2003).
[7] J. M. Gérard, B. Sermage, B. Gayral, E. Costard, and V. Thierry-Mieg, Enhanced spontaneous emission by quantum boxes in a monolithic optical microcavity, Phys. Rev. Lett. **81**, 1110–1113 (1998).
[8] J. P. Reithmaier, G. Sek, A. Löffler, C. Hofmann, S. Kuhn, S. Reitzenstein, L. V. Keldysh, V. D. Kulakovskii, T. L. Reinecke, and A. Forchel, Strong coupling in a single quantum dot-semiconductor microcavity system, Nature **432**, 197–200 (2004).
[9] T. Yoshie, A. Scherer, J. Hendrickson, G. Khitrova, H. M. Gibbs, G. Rupper, C. Ell, O. B. Shchekin, and D. G. Deppe, Vacuum Rabi splitting with a single quantum dot in a photonic crystal nanocavity, Nature **432**, 200–203 (2004).
[10] Q. Xu, P. Dong, and M. Lipson, Breaking the delay-bandwidth product in a photonic structure, Nature Phys. **3**, 406–410 (2007).
[11] B. E. Little, H. A. Haus, J. S. Foresi, L. C. Kimerling, E. P. Ippen, and D. J. Ripin, Wavelength switching and routing using absorption and resonance, IEEE Photonics Technol. Lett. **10,** 816–818 (1998).
[12] F. Xia, L. Sekaric, and Y. Vlasov, Ultracompact optical buffers on a silicon chip, Nature Photonics **1**, 65–71 (2007).
[13] M. Notomi, T. Tanabe, A. Shinya, E. Kuramochi, H. Taniyama, S. Mitsugi, and M. Morita, Nonlinear and adiabatic control of high-Q photonic crystal nanocavities, Opt. Express **26**, 17458–17481 (2007).
[14] A. Sciuto, S. Libertino, A. Alessandria, S. Coffa, and G. Coppola, Design, fabrication, and testing of an integrated Si-based light modulator, J. Lightwave Technol. **21**, 228–235 (2003).
[15] Q. Xu, B. Schmidt, S. Pradhan, and M. Lipson, Micrometre-scale silicon electro-optic modulator, Nature **435**, 325–327 (2005).
[16] J. P. Zhang, D. Y. Chu, S. V. Wu, S. T. Ho, W. G. Bi, C. W. Tu, and R. C. Tiberio, Photonic-wire laser, Phys. Rev. Lett. **75**, 2678–2681 (1995).
[17] H. G. Park, S. H. Kim, S. H. Kwon, Y. G. Ju, J. K. Yang, J. H. Baek, S. B. Kim, and Y. H. Lee, Electrically driven single-cell photonic crystal laser, Science **305**, 1444–1447 (2004).
[18] K. Nozaki, S. Kita, and T. Baba, Room temperature continuous wave operation and controlled spontaneous emission in ultrasmall photonic crystal nanolaser, Opt. Express **15**, 7506–7514 (2007).

[19] K. Nozaki, H. Watanabe, and T. Baba, Photonic crystal nanolaser monolithically integrated with passive waveguide for effective light extraction, Appl. Phys. Lett. **92**, 021108 (2008).
[20] A. M. Armani, R. P. Kulkarni, S. E. Fraser, R. C. Flagan, and K. J. Vahala, Label-free, single molecule detection with optical microcavities, Science **317**, 783–786 (2007).
[21] K. Iga, F. Koyama, and S. Kinoshita, Surface emitting semiconductor-lasers, IEEE J. Quantum Electron. **24**, 1845–1855 (1988).
[22] S. Reitzenstein, C. Hofmann, A. Gorbunov, M. Gorbunov, M. Strauss, S. H. Kwon, C. Schneider, A. Löffler, S. Hoefling, M. Kamp, and A. Forchel, AlAs/GaAs micropillar cavities with quality factors exceeding 150,000, Appl. Phys. Lett. **90**, 251109 (2007).
[23] G. Lecamp, J. P. Hugonin, P. Lalanne, R. Braive, S. Varoutsis, S. Laurent, A. Lemaître, I. Sagnes, G. Patriarche, I. Robert-Philip, and I. Abram, Submicron-diameter semiconductor pillar microcavities with very high quality factors, Appl. Phys. Lett. **90**, 091120 (2007).
[24] J. P. Zhang, D. Y. Chu, S. L. Wu, W. G. Bi, R. C. Tiberio, R. M. Joseph, A. Taflove, C. W. Tu, and S. T. Ho, Nanofabrication of 1-D photonic bandgap structures along a photonic wire, IEEE Photonics Technol. Lett. **8**, 491–93 (1996).
[25] J. S. Foresi, P. R. Villeneuve, J. Ferrera, E. R. Thoen, G. Steinmeyer, S. Fan, J. D. Joannopoulos, L. C. Kimerling, H. I. Smith, and E. P. Ippen, Photonic-bandgap microcavities in optical waveguides, Nature **390**, 143–145 (1997).
[26] P. Velha, J. C. Rodier, P. Lalanne, J. P. Hugonin, D. Peyrade, and E. Hadji, Ultra-high-reflectivity photonic-bandgap mirrors in a ridge SOI waveguide, New J. Phys. **8**, 204 (2006).
[27] J. D. Joannopoulos, R. D. Meade, and J. N. Winn, Photonic Crystals (Princeton University Press, 1995).
[28] Y. Akahane, T. Asano, B. S. Song, and S. Noda, High-Q photonic nanocavity in two-dimensional photonic crystal, Nature **425**, 944–947 (2003).
[29] E. Weidner, S. Combrie, N. V. Q. Tran, A. De Rossi, J. Nagle, S. Cassette, A. Talneau, and H. Benisty, Achievement of ultrahigh quality factors in GaAs photonic crystal membrane nanocavity, Appl. Phys. Lett. **89**, 221104 (2006).
[30] S. G. Johnson, S. Fan, A. Mekis, and J. D. Joannopoulos, Multipole-cancellation mechanism for high-Q cavities in the absence of a complete photonic band gap, Appl. Phys. Lett. **78**, 3388–3390 (2001).
[31] J. Vuckovic, M. Pelton, A. Scherer, and Y. Yamamoto, Optimization of three-dimensional micropost microcavities for cavity quantum electrodynamics, Phys. Rev. A **66**, 023808 (2002).
[32] J. Vuckovic, M. Loncar, H. Mabuchi, and A. Scherer, Optimization of the Q factor in photonic crystal microcavities, IEEE J. Quantum Electron. **38**, 850–856 (2002).
[33] K. Srinivasan and O. Painter, Momentum space design of high-Q photonic crystal optical cavities, Opt. Express **10**, 670–684 (2002).
[34] P. Lalanne, S. Mias, and J. P. Hugonin, Two physical mechanisms for boosting the quality factor to cavity volume ratio of photonic crystal microcavities, Opt. Express **12**, 458–467 (2004).
[35] D. Englund, I. Fushman, and J. Vuckovic, General recipe for designing photonic crystal cavities, Opt. Express **13**, 5961–5975 (2005).
[36] J. Goh, I. Fushman, D. Englund, and J. Vuckovic, Genetic optimization of photonic bandgap structures, Opt. Express **15**, 8218–8230 (2007).
[37] J. D. Jackson, Classical Electrodynamics, 2nd ed, (John Wiley, New York, 1974).
[38] A. W. Snyder and J. D. Love, Optical Waveguide Theory (Chapman and Hall, New York, 1983).
[39] H. Benisty, Photonic crystals: New designs to confine light, Nature Phys. **1**, 9–10 (2005).
[40] M. Palamaru and P. Lalanne, Photonic crystal waveguides: out-of-plane losses and adiabatic modal conversion, Appl. Phys. Lett. **78**, 1466–1469 (2001).
[41] H. A. Haus, Waves and Fields in Optoelectronics (Prentice-Hall International, London, 1984).
[42] J. P. Hugonin and P. Lalanne, Perfectly matched-layers as nonlinear coordinate transforms: a generalized formalization, J. Opt. Soc. Am. A. **22**, 1844–49 (2005).
[43] G. Lecamp, J. P. Hugonin, and P. Lalanne, Theoretical and computational concepts for periodic optical waveguides, Opt. Express **15**, 11042–11060 (2007).
[44] C. Sauvan, P. Lalanne, and J. P. Hugonin, Tuning holes in photonic-crystal nanocavities, Nature **429**, doi:10.1038/nature02602 (2004).
[45] C. Sauvan, P. Lalanne, and J. P. Hugonin, Slow-wave effect and mode-profile matching in photonic crystal microcavities, Phys. Rev. B **71**, 165118 (2005).
[46] P. Lalanne and J. P. Hugonin, Bloch-wave engineering for high Q's, small V's microcavities, IEEE J. Quantum Electron. **39**, 1430–38 (2003).
[47] C. Sauvan, G. Lecamp, P. Lalanne, and J. P. Hugonin, Modal-reflectivity enhancement by geometry tuning in photonic crystal microcavities, Opt. Express **13**, 245–255 (2005).
[48] J. Ctyroky, Photonic bandgap structures in planar waveguides, J. Opt. Soc. Am. A **18**, 435–441 (2001).
[49] T. F. Krauss and R. M. De La Rue, Optical characterization of waveguide based photonic microstructures, Appl. Phys. Lett. **68**, 1613–1615 (1996).
[50] T. Baba, M. Hamasaki, N. Watanabe, P. Kaewplung, A. Matsutani, T. Mukaihara, F. Koyama, and K. Iga, A novel short-cavity laser with deep-grating distributed Bragg reflectors, Jpn. J. Appl. Phys. **35**, 1390–1394 (1996).
[51] T. F. Krauss, O. Painter, A. Scherer, J. S. Roberts, and R. M. De La Rue, Photonic microstructures as laser mirrors, Opt. Eng. **37**, 1143–1148 (1998).
[52] D. Peyrade, E. Silberstein, P. Lalanne, A. Talneau, and Y. Chen, Short Bragg mirrors with adiabatic modal conversion, Appl. Phys. Lett. **81**, 829–831 (2002).
[53] B. Cluzel, E. Picard, T. Charvolin, E. Hadji, L. Lalouät, F. de, Fornel, C. Sauvan, and P. Lalanne, Near-field spectroscopy of low-loss waveguide integrated microcavities, Appl. Phys. Lett. **88**, 051112 (2006).
[54] P. Velha, J. C. Rodier, P. Lalanne, J. P. Hugonin, D. Peyrade, E. Picard, T. Charvolin, and E. Hadji, Ultra-compact SOI ridge-waveguide mirrors with high reflectance, Appl. Phys. Lett. **89**, 171121 (2006)
[55] P. Velha, E. Picard, E. Hadji, J. C. Rodier, P. Lalanne, and D. Peyrade, Ultrahigh Q/V Fabry-Perot microcavity on SOI substrate, Opt. Express **15**, 16090–16096 (2007).
[56] A. R. Md Zain, M. Gnan, H. M. H. Chong, M. Sorel, and R. M. De La Rue, Tapered photonic crystal microcavities

embedded in photonic wire waveguides with large resonance quality-factor and high transmission, IEEE Photonics Technol. Lett. **20**, 6–8 (2008).
[57] A. R. Md Zain, N. P. Johnson, M. Sorel, and R. M. De La Rue, Ultra high quality factor one dimensional photonic crystal/photonic wire micro-cavities in silicon-on-insulator (SOI), Opt. Express **16**, 12084–12089 (2008).
[58] Y. Akahane, T. Asano, B. S. Song, and S. Noda, Fine-tuned high-Q photonic-crystal, Opt. Express **13**, 1202–1214 (2005).
[59] B. S. Song, S. Noda, T. Asano, and Y. Akahane, Ultra-high-Q photonic double-heterostructure nanocavity, Nature Mater. **4**, 207–210 (2005).
[60] E. Kuramochi, M. Notomi, S. Mitsugi, A. Shinya, T. Tanabe, and T. Watanabe, Ultrahigh-Q photonic crystal nanocavities realized by the local width modulation of a line defect, Appl. Phys. Lett. **88**, 041112 (2006).
[61] T. Tanabe, M. Notomi, E. Kuramochi, A. Shinya, and H. Taniyama, Trapping and delaying photons for one nanosecond in an ultrasmall high-Q photonic crystal nanocavity, Nature Photonics **1**, 49–52 (2007).
[62] X. Yang and C. W. Wong, Design of photonic band gap nanocavities for stimulated Raman amplification and lasing in monolithic silicon, Opt. Express **13**, 4723–4730 (2005).
[63] F. Bordas, M. J. Steel, C. Seassal, and A. Rahmani, Confinement of band-edge modes in a photonic crystal slab, Opt. Express **15**, 10890–10902 (2007).
[64] L. Ferrier, X. Letartre, P. Rojo-Romeo, E. Drouard, and P. Vicktorovitch, Slow Bloch mode confinement in 2D photonic crystals for surface operating devices, Opt. Express **16**, 3136–3145 (2008).
[65] http://www.virgo.infn.it/.
[66] L. A. Coldren and S. W. Corzine, Diode lasers and photonic integrated circuits (J. Wiley and Sons, New York, 1995).
[67] F. Riboli, A. Recati, N. Daldosso, L. Pavesi, G. Pucker, A. Lui, S. Cabrini, and E. Di, Fabrizio, Photon recycling in Fabry-Perot micro-cavities based on Si_3N_4 waveguides, Photonics Nanostruct. Fund. Applic. **4**, 41–46 (2006).
[68] P. Velha, Ingénierie de mode en optique intégrée sur silicium sur isolant, PhD dissertation thesis in French, Orsay University (2008).
[69] H. G. Park, J. K. Hwang, J. Huh, H. Y. Ryu, Y. H. Lee, and J. S. Kim, Nondegenerate monopole-mode two-dimensional photonic band gap laser, Appl. Phys. Lett. **79**, 3032–3034 (2001).
[70] L. A. Graham, D. L. Huffaker, and D. G. Deppe, Spontaneous lifetime control in a native-oxide-apertured microcavity, Appl. Phys. Lett. **74**, 2408–2410 (1999).
[71] G. Solomon, M. Pelton, and Y. Yamamoto, Single-mode spontaneous emission from a single quantum dot in a three-dimensional microcavity, Phys. Rev. Lett. **86**, 3903–3906 (2001).
[72] P. Lalanne, J. P. Hugonin, and J. M. Gérard, Electromagnetic study of the Q of pillar microcavities in the small limit diameter, Appl. Phys. Lett. **84**, 4726–28 (2004).
[73] J. M. Gérard, Solid-state cavity quantum electrodynamics with self-assembled quantum dots, in: Single Quantum Dots: Physics and Applications (Springer, Heidelberg, 2003).
[74] G. Lecamp, P. Lalanne, J. P. Hugonin, and J. M. Gérard, Energy transfer through laterally confined Bragg Mirrors and its impact on pillar microcavities, IEEE J. Quantum Electron. **41**, 1323–1329 (2005).
[75] M. Soljacic and J. D. Joannopoulos, Enhancement of nonlinear effects using photonic crystals, Nature Mater. **3**, 211–219 (2004).
[76] J. T. Robinson, C. Manolatou, L. Chen, and M. Lipson, Ultrasmall mode volumes in dielectric optical microcavities, Phys. Rev. Lett. **95**, 143901 (2005).
[77] S. A. Maier, Plasmonics field enhancement and SERS in the effective mode volume picture, Opt. Express **14**, 1957–1964 (2006).
[78] D. Gerace and L. C. Andreani, Effect of disorder on propagation losses and cavity Q-factors in photonic crystal slabs, Photonics Nanostruct. Fund. Appl. **3**, 120–128 (2005).